

pubs.acs.org/JPCL Letter

# Data-Driven Refinement of Electronic Energies from Two-Electron Reduced-Density-Matrix Theory

Grier M. Jones, Run R. Li, A. Eugene DePrince, III,\* and Konstantinos D. Vogiatzis\*



Cite This: J. Phys. Chem. Lett. 2023, 14, 6377-6385



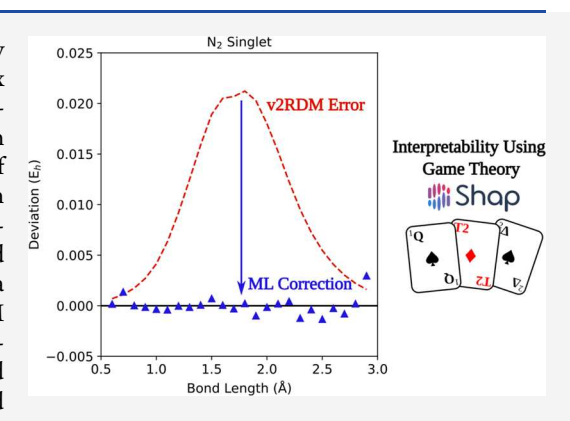
**ACCESS** I

III Metrics & More

Article Recommendations

s Supporting Information

**ABSTRACT:** The exponential computational cost of describing strongly correlated electrons can be mitigated by adopting a reduced-density matrix (RDM)-based description of the electronic structure. While variational two-electron RDM (v2RDM) methods can enable large-scale calculations on such systems, the quality of the solution is limited by the fact that only a subset of known necessary *N*-representability constraints can be applied to the 2RDM in practical calculations. Here, we demonstrate that violations of partial three-particle (T1 and T2) *N*-representability conditions, which can be evaluated with knowledge of only the 2RDM, can serve as *physics-based* features in a machine-learning (ML) protocol for improving energies from v2RDM calculations that consider only two-particle (PQG) conditions. Proof-of-principle calculations demonstrate that the model yields substantially improved energies relative to reference values from configuration-interaction-based calculations.



An active space of strongly correlated electrons is challenging to describe computationally because the complexity of the exact configuration interaction (CI) wave function grows exponentially with the number of active electrons and orbitals. As a result, the largest reported complete active space self-consistent field (CASSCF)<sup>1-4</sup> calculation to date involved only 22 electrons distributed among 22 orbitals [a (22e, 22o) active space].<sup>5</sup> In light of these difficulties, a large body of work has attempted to circumvent the exponential scaling of exact CI through various approximate CI schemes, 6-14 as well as via alternative representations of the electronic structure, including the density matrix renormalization group (DMRG) approach and two-electron reduced density matrix (2RDM) methods. 20,21

The energy of a many-electron system can be represented exactly in terms of the 2RDM, and the 2RDM itself is a compact mathematical object (relative to the complexity of the wave function). Hence, a 2RDM-based representation of electronic structure seems natural, ostensibly making 2RDM theory a desirable alternative to CI. Unfortunately, a variety of issues plague 2RDM-based calculations, <sup>22–27</sup> and these issues are rooted in a singular challenge: without explicit knowledge of a wave function that maps to the 2RDM, a large number of nontrivial constraints must be applied to the 2RDM to guarantee that it is derivable from an *N*-electron density matrix or an ensemble of such density matrices. Such a 2RDM is said to be "*N*-representable."

The ensemble N-representability problem is, in principle, solved, at least in the sense that a complete hierarchy of

constraints on the 2RDM has been proposed.<sup>29-31</sup> In practical variational 2RDM (v2RDM) calculations, 20-24,26,32-56 however, one imposes only a subset of necessary N-representability conditions; such conditions usually include the two-particle (PQG) conditions<sup>35</sup> or the partial three-particle conditions known as T1 and T2. 44,57 At the PQG level, in particular, large numbers of strongly correlated electrons can be efficiently treated; for example, a v2RDM-based calculation involving a (64e, 64o) active space can be completed in a matter of hours.<sup>55</sup> While PQG-level calculations can give important insight into the qualitative properties of strongly correlated systems, the quantitative accuracy of such calculations can be poor, with the correlation energy often overestimated by as much as 20%, even in small systems near their equilibrium geometries.<sup>58</sup> PQG-derived energy differences, such as spinstate splittings,<sup>21</sup> can be much more accurate, but it is nonetheless clear that partial three-particle conditions (e.g., T2) or even full three-particle conditions (three-positivity or 3POS)<sup>43,59</sup> may be necessary to achieve quantitative accuracy, in general. The challenge is that imposing these additional conditions comes at a much higher floating-point cost.

Received: May 19, 2023 Accepted: July 3, 2023 Published: July 7, 2023





Machine learning (ML) is an emerging tool in electronic structure theory for recovering the electronic energies, 60–67 wave functions, 68,69 and molecular properties of post-Hartree–Fock methods. To Specifically, for ML applications to wave function methods, representative examples include coupled-cluster with singles-and-doubles excitations (CCSD), where ML is used to learn the two-electron amplitudes, 65,68 and the CI problem where ML allows the efficient selection of important configurations. With respect to RDMs, a so-called density tensor representation has been proposed to predict CCSD electronic energies and dipole moments from the one-electron reduced density matrix (1RDM), and more recently, Sager-Smith and Mazziotti have demonstrated that geminal occupations (the eigenvalues of the 2RDM) can be estimated from correlation temperatures extracted from a convolutional neural network.

The goal of the present work is the prediction of complete active space (CAS) CI quality electronic energies from CASv2RDM calculations that consider only the PQG constraints. Toward this aim, we developed an ML protocol called datadriven v2RDM (DDv2RDM) that learns differences between CI and v2RDM energies using features that can be generated from RDMs optimized at the PQG level of theory. Crucial to the success of this model is the recognition that the T1 and T2 conditions are partial three-particle conditions, in the sense that they are expressible in terms of the 2RDM, without knowledge of any three-body RDMs. As such, violations of the T1 and T2 conditions can be evaluated using 2RDMs generated at the PQG level of theory. Here, we show that these intrinsic features of the v2RDM method are necessary for a transferable ML model. Moreover, this procedure paves the way for improved data-driven v2RDM models that consider additional higher-order lifted constraints<sup>29,31</sup> that also only depend on the 2RDM and, thus, could serve as features in such ML-based models.

The elements of the 1RDM and the 2RDM are defined in second-quantized form as

$${}^{1}D_{q_{\sigma}}^{p_{\sigma}} = \langle \Psi | \hat{a}_{p_{\sigma}}^{\dagger} \hat{a}_{q_{\sigma}} | \Psi \rangle \tag{1}$$

and

$$^{2}D_{r_{\sigma}s_{\tau}}^{p_{\sigma}q_{\tau}} = \langle \Psi | \hat{a}_{p_{\sigma}}^{\dagger} \hat{a}_{q_{\tau}}^{\dagger} \hat{a}_{s_{\tau}} \hat{a}_{r_{\sigma}} | \Psi \rangle$$
 (2)

respectively. Here, indices p, q, r, and s represent spatial molecular orbital labels and  $\sigma$  and  $\tau$  are spin labels. We are considering only nonrelativistic Hamiltonians, in which case the nonzero blocks of  ${}^1\mathbf{D}$  and  ${}^2\mathbf{D}$  are spin conserving. In order for the 2RDM to be physically meaningful, it must satisfy a number of statistical conditions: it should have a fixed trace, be Hermitian, be antisymmetric with respect to the exchange of particle labels, and contract to the 1RDM. These RDMs must also be positive semidefinite (e.g.,  ${}^2\mathbf{D} \succeq 0$ ). At the PQG level of theory, the one-hole RDM ( ${}^1\mathbf{Q}$ ), the two-hole RDM ( ${}^2\mathbf{Q}$ ), and the particle-hole RDM ( ${}^2\mathbf{G}$ ) should also be positive semidefinite, and the elements of these RDMs should map onto the elements of the 2RDM and 1RDM according to the anticommutation relations of Fermionic creation and annihilation operators. The elements of  ${}^1\mathbf{Q}$ ,  ${}^2\mathbf{Q}$ , and  ${}^2\mathbf{G}$  are defined as

$${}^{1}Q_{q_{\sigma}}^{p_{\sigma}} = \langle \Psi | \hat{a}_{p_{\sigma}} \hat{a}_{q_{\sigma}}^{\dagger} | \Psi \rangle \tag{3}$$

$${}^{2}Q_{r_{\sigma}s_{\tau}}^{p_{\sigma}q_{\tau}} = \langle \Psi | \hat{a}_{p_{\sigma}}\hat{a}_{q_{\tau}}\hat{a}_{s_{\tau}}^{\dagger}\hat{a}_{r_{\sigma}}^{\dagger} | \Psi \rangle \tag{4}$$

and

$${}^{2}G_{r_{s}s_{i}}^{p_{\sigma}q_{\tau}} = \langle \Psi | \hat{a}_{p_{s}}^{\dagger} \hat{a}_{q_{s}} \hat{a}_{s_{i}}^{\dagger} \hat{a}_{r_{k}} | \Psi \rangle \tag{5}$$

respectively. Here, we see that  ${}^1\mathbf{Q}$  and  ${}^2\mathbf{Q}$  have the same spinblock structures as  ${}^1\mathbf{D}$  and  ${}^2\mathbf{D}$ , respectively, whereas that of  ${}^2\mathbf{G}$  is more complex. The symbols  $\kappa$  and  $\lambda$  represent spin labels, and the nonzero spin blocks of  ${}^2\mathbf{G}$  are those for which the number of  $\alpha$ -spin ( $\beta$ -spin) creation operators equals the number of  $\alpha$ -spin ( $\beta$ -spin) annihilation operators.

At the full 3POS level of theory, four additional three-body RDMs should be positive semidefinite and map to one another and to the 2RDM (see ref 59 for additional details). The elements of these RDMs are defined by

$${}^{3}D_{s_{\sigma}t_{r}u_{\kappa}}^{p_{\sigma}q_{r}r_{\kappa}} = \langle \Psi | \hat{a}_{p_{\sigma}}^{\dagger} \hat{a}_{q_{r}}^{\dagger} \hat{a}_{r_{\kappa}}^{\dagger} \hat{a}_{u_{\kappa}} \hat{a}_{t_{r}} \hat{a}_{s_{\sigma}} | \Psi \rangle \tag{6}$$

$${}^{3}E^{p_{\sigma}q_{\tau}r_{\kappa}}_{s_{\lambda}t_{\mu}u_{\nu}} = \langle \Psi | \hat{a}^{\dagger}_{p_{\sigma}}\hat{a}^{\dagger}_{q_{\tau}}\hat{a}_{r_{\kappa}}\hat{a}^{\dagger}_{u_{\mu}}\hat{a}_{t_{\mu}}\hat{a}_{s_{\lambda}} | \Psi \rangle \tag{7}$$

$${}^{3}F^{p_{r}q_{z}r_{\kappa}}_{s_{\lambda}t_{\mu}u_{\nu}} = \langle \Psi | \hat{a}^{\dagger}_{u_{\nu}}\hat{a}_{t_{\mu}}\hat{a}_{s_{\lambda}}\hat{a}^{\dagger}_{p_{\sigma}}\hat{a}^{\dagger}_{q_{\tau}}\hat{a}_{r_{\kappa}} | \Psi \rangle \tag{8}$$

and

$${}^{3}Q_{s_{\sigma}t_{\tau}u_{\kappa}}^{p_{\sigma}q_{\tau}r_{\kappa}} = \langle \Psi | \hat{a}_{p_{\sigma}}\hat{a}_{q_{\tau}}\hat{a}_{r_{\kappa}}\hat{a}_{u_{\kappa}}^{\dagger}\hat{a}_{t_{\tau}}^{\dagger}\hat{a}_{s_{\sigma}}^{\dagger} | \Psi \rangle \tag{9}$$

Here,  $\mu$  and  $\nu$  represent spin functions, and as was the case for  ${}^2\mathbf{G}$ , the nonzero spin blocks of  ${}^3\mathbf{E}$  and  ${}^3\mathbf{F}$  are those for which the number of  $\alpha$ -spin ( $\beta$ -spin) creation operators equals the number of  $\alpha$ -spin ( $\beta$ -spin) annihilation operators. One can also define weaker three-body constraints on the 2RDM by taking specific linear combinations of the three-particle RDMs defined above. In particular, we have

$$\mathbf{T1} = {}^{3}\mathbf{D} + {}^{3}\mathbf{Q} \tag{10}$$

$$\mathbf{T2} = {}^{3}\mathbf{E} + {}^{3}\mathbf{F} \tag{11}$$

Both of these RDMs should be positive semidefinite, and importantly, the right-hand sides of eqs 10 and 11 can be defined without knowledge of any three-body RDM. As a result, we can evaluate errors in the T1 and T2 conditions (the appearance of negative eigenvalues in these matrices) using RDMs optimized at the PQG level of theory.

The aim of our work is to develop an ML model to learn the difference between CI energies and those generated at the PQG level of theory using features based on the RDMs defined above. In order to generate a viable and transferable model, we performed extensive exploratory data analysis and feature engineering. We include the following features in the DDv2RDM model: the entropy of one- and two-body RDMs

$$S = \sum_{i} n_i \log_2 n_i \tag{12}$$

where  $n_i$  are the eigenvalues of the RDM, traces of the spin blocks of the cumulant 2RDM,  $Tr(^2\Delta)$ , with

$$^{2}\Delta = ^{2}\mathbf{D} - ^{1}\mathbf{D} \wedge ^{1}\mathbf{D} \tag{13}$$

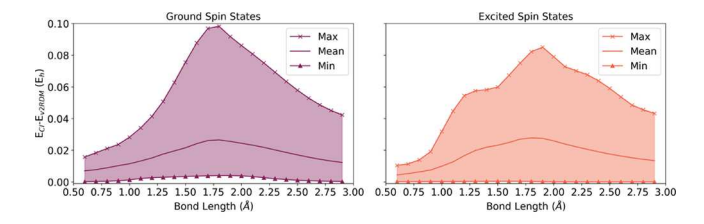
the norms of the spin blocks of the cumulant 2RDM,  $\|^2\Delta\|^2$ , and information related to violations in the T1 and T2 conditions (i.e., the existence of negative eigenvalues). We quantify both the frequency of the T1 and T2 violations (how many eigenvalues are negative, as a percentage) as well as the

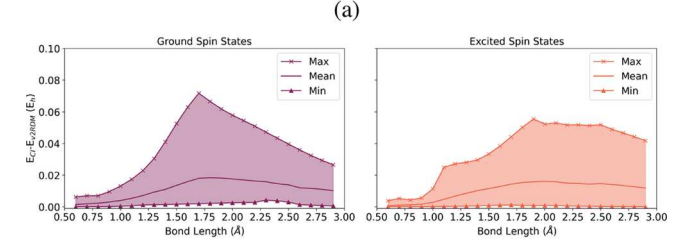
magnitude and distribution of these violations (average, variance, and root-mean-square of the negative eigenvalues). In eq 13, the symbol  $\land$  denotes the Grassman wedge product.<sup>79</sup>

Our data set includes these features computed along potential energy curves for 36 neutral diatomic species formed from hydrogen, lithium, beryllium, boron, carbon, nitrogen, oxygen, and fluorine atoms. We consider multiple spin states, i.e., singlet and triplet states for molecules with even numbers of active electrons and doublet and quartet states for molecules with odd numbers of active electrons. Dissociation curves are evaluated over interatomic distances ranging from 0.6 to 2.9 Å for all cases. We also considered multiple basis sets (STO-3G, 6-31G, and cc-pVDZ). For minimal basis (STO-3G) calculations, the active space was chosen to be the full orbital space, whereas correlated calculations performed within the 6-31G and cc-pVDZ basis sets considered only the full valence space to be active. Canonical restricted (open-shell) Hartree-Fock orbitals were used in all correlated calculations (i.e., the orbitals were not further optimized for v2RDM- or CI-driven CASSCF). All v2RDM calculations account for PQG<sup>35</sup> ensemble N-representability constraints. The v2RDM calculations were considered converged when the primal-dual energy gap fell below  $10^{-6}$   $E_{\rm h}$  and the primal/dual errors fell below 10<sup>-5</sup>. We refer the reader to ref 55 for a description of these quantities. We used a value of  $-1 \times 10^{-8}$  for eigenvalues of T1 and T2 as a cutoff when evaluating the statistical measures of violations in these conditions.

In our ML model, we formulate the target value as a correction to the v2RDM energy, i.e., the difference between the CI and v2RDM energies,  $E_{\rm CI}-E_{\rm v2RDM}$ . Systems for which the mean of the root-mean-square errors (RMSEs) of the T1 or T2 violations across the potential energy curve are less than  $10^{-6}$  are excluded. Since we consider multiple spin states, the ML model is evaluated on two sets of data, corresponding to systems in their ground or excited spin states, as determined by the CI energy at the equilibrium geometry. The spin multiplicities for all systems can be found in the Supporting Information (Figure S1).

To gain insights into the distributions of the target values, we analyze the minimum, mean, and maximum values across the potential energy curves for all molecules represented within the STO-3G, 6-31G, and cc-pVDZ basis sets (Figure 1a,b,c, respectively). As shown in Figure 1a-c, the maximum deviation often occurs at intermediate bond lengths, with the exception of the ground spin states optimized in the cc-pVDZ basis (left-hand panel of Figure 1c). In this case, the maximum deviation occurs closer to the bond dissociation limit. For the ground spin states, the maximum deviation between v2RDM and CI energies occurs for the singlet state of the C2 molecule, regardless of the basis set. For the STO-3G, 6-31G, and ccpVDZ basis sets, these maximum deviations are 0.0982  $E_{\rm h}$ ,  $0.0717 E_{\rm h}$ , and  $0.0485 E_{\rm h}$ , respectively. For the excited spin states, the maximum deviation between v2RDM and CI energies occurs for the doublet state of the BC molecule in the STO-3G and 6-31G basis sets and the singlet state of the BN molecule in the cc-pVDZ basis set. For the STO-3G, 6-31G, and cc-pVDZ basis sets, these maximum deviations are 0.0850  $E_{\rm h}$ , 0.0554  $E_{\rm h}$ , and 0.06179  $E_{\rm h}$ , respectively. Overall, these large deviations between the CI and v2RDM energies motivate the development of an ML-based methodology to correct the v2RDM energies.





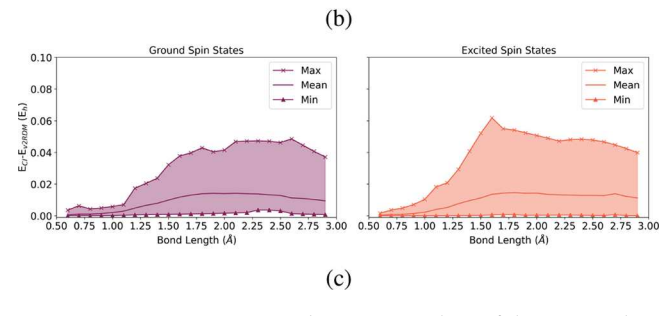


**Figure 1.** Minimum, mean, and maximum values of the target values  $(E_{\text{CI}} - E_{\text{V2RDM}})$  at each bond length for ground (left) and excited (right) spin states optimized within the (a) STO-3G, (b) 6-31G, and (c) cc-pVDZ basis sets.

All ML models developed for this study utilize kernel ridge regression (KRR) with a radial basis function (RBF) kernel, defined as

$$k(x_i, x_j) = \exp(-\gamma ||x_i - x_j||_2^2)$$
(14)

where  $\gamma$  is a hyperparameter. In all models, input features were normalized using a MinMaxScaler function, while  $\gamma$  and the model regularization parameter  $\alpha$  were optimized using a 5-fold parameter grid search as implemented in Sci-kit Learn. An example of the model parameters examined can be found in the Supporting Information (section S2).

Figure 2 shows CI and v2RDM potential energy curves (panel a) as well as deviations between CI energies and those from v2RDM and DDv2RDM (panel b) for a representative example: the N<sub>2</sub> molecule within the cc-pVDZ basis set. Here, we consider evenly spaced points along the curves, with 50% of the data used for training and the remaining data reserved for testing. Figure 2b shows that the maximum deviation between CI and v2RDM for the singlet state is  $2.1222 \times 10^{-2} E_h$  at 1.8 Å, while that for the triplet state is  $1.7031 \times 10^{-2} E_h$  at 1.7 Å. Overall, the RMSE between CI and v2RDM energies are  $1.2149 \times 10^{-2} E_{\rm h}$  and  $9.6136 \times 10^{-3} E_{\rm h}$  for the ground and excited states, respectively. Addition of the DDv2RDM correction reduces the RMSE of the singlet spin state to  $2.3550 \times 10^{-4} E_h$  and  $1.1683 \times 10^{-3} E_h$  for the training and test sets, respectively. For the triplet spin state, the training set RMSE is reduced to  $7.0262 \times 10^{-9} E_{\rm h}$ , while for the test set the error is reduced to  $8.8469 \times 10^{-4} E_{\rm h}$ . These reductions translate into percent improvements of 98.1% and 90.3% for the training and testing for the singlet state, respectively, while

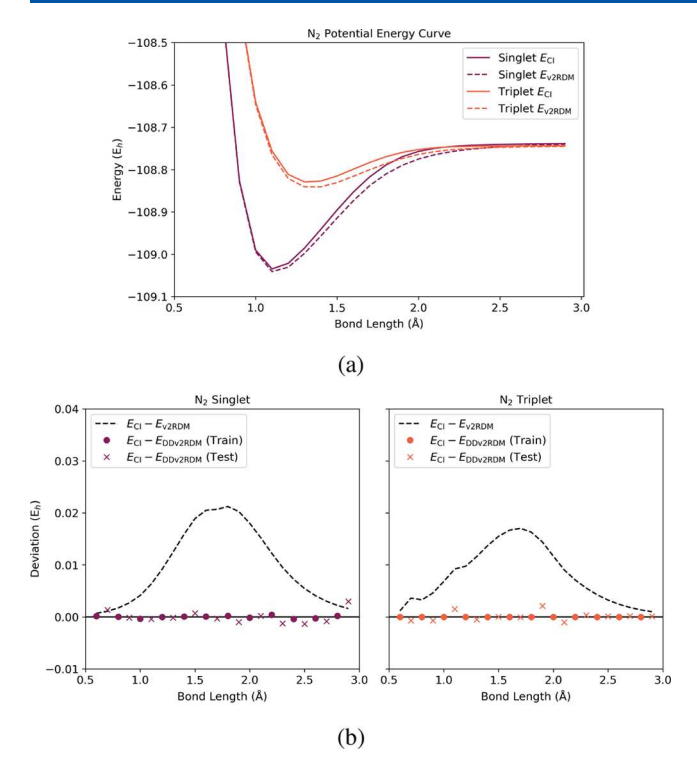


Figure 2. (a) The potential energy curves of  $N_2$  using the cc-pVDZ basis set for the ground (singlet, purple) and excited (triplet, orange) spin states. The CI energy is shown as a solid line and the v2RDM energy as a dashed line. (b) Deviations between CI and (DD)v2RDM energies.

for the triplet state, these improvements are 99.9% and 90.8%, respectively.

We have assessed the transferability of the DDv2RDM method for two cases: (i) different models were developed for ground versus excited spin states within a given basis set, and (ii) a unified model was created that considered all available data within a given basis set. Based on the T1/T2 selection criteria, the data set for the ground spin states includes 22 STO-3G, 17 6-31G, and 18 cc-pVDZ systems, while that for the excited spin states includes 19 STO-3G, 21 6-31G, and 19 cc-pVDZ systems. We evaluate the performance of the models using standard regression metrics, which include the RMSE and the coefficient of determination  $(R^2)$ . It was found that the most transferable and least overfit model was obtained when both sets of data were used for training and testing DDv2RDM (section S4 in the Supporting Information). The regression parity plots for this model are shown in Figure 3 for the three basis sets under consideration. For the STO-3G basis set (Figure 3a), the model achieves  $R^2$  values of 0.9891 and 0.9858 for the training and test set, respectively. The training set has an RMSE of 1.8393  $\times$  10<sup>-3</sup>  $E_{\rm h}$ , and the test set has an RMSE of  $2.1117 \times 10^{-3} E_{\rm h}$ . Figure 3 shows that the model trained on 6-31G data exhibits increased accuracy, with respect to the STO-3G basis set. Training and testing  $R^2$  values are 0.9954 and 0.9897, respectively, which correspond to RMSE values of  $8.8163 \times 10^{-4} E_{\rm h}$  and  $1.3442 \times 10^{-3} E_{\rm h}$ , respectively. The least overfit model is the cc-pVDZ model (Figure 3), which has  $R^2$ values of 0.9468 and 0.9426 for training and testing, respectively, with RMSEs of 2.6844  $\times$  10<sup>-3</sup>  $E_h$  and 2.7863  $\times$  $10^{-3} E_{\rm h}$ , respectively.

We further examined the performance of our model by analyzing the RMSE of the DDv2RDM energy for each system

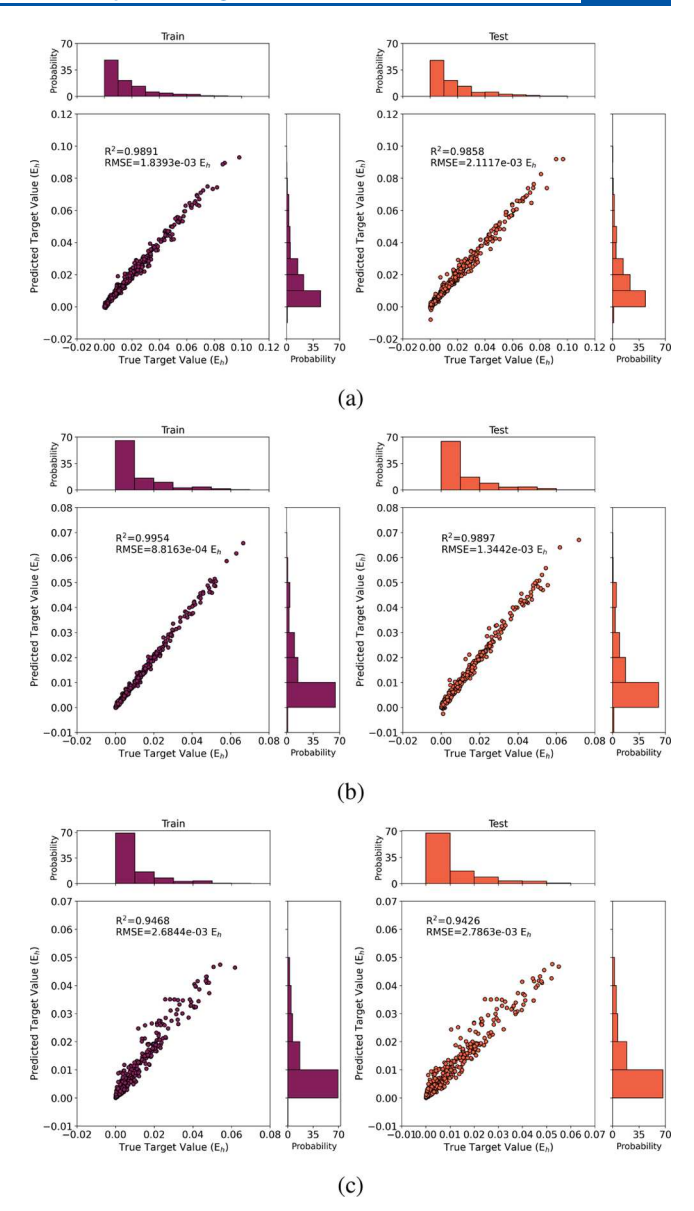
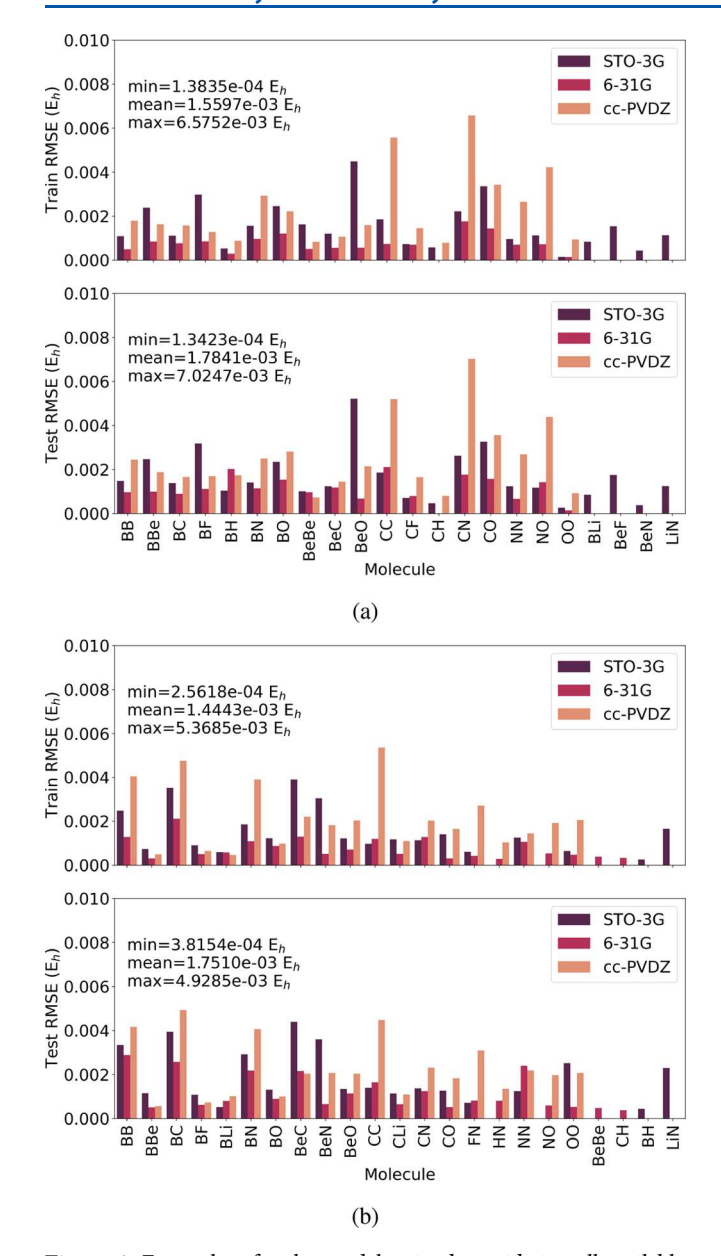


Figure 3. Regression parity plots comparing the true, calculated target values with the predicted target values for the (a) STO-3G, (b) 6-31G, and (c) cc-pVDZ basis sets. Probability density histograms are given on the x- and y-axes. The left (purple) panel shows the training and right (orange) panel shows the test data.

in the ground and excited spin states, as shown in Figure 4. For the STO-3G basis set, the molecules with the largest training and test errors are the singlet (ground) state of BeO (4.4841 ×  $10^{-3}E_{\rm h}$  and 5.2121  $\times$   $10^{-3}$   $E_{\rm h}$ , respectively, Figure 4a) and the singlet (excited) state of BeC (3.8980  $\times$  10<sup>-3</sup>  $E_h$  and 4.3875  $\times$  $10^{-3}E_{\rm h}$ , respectively, Figure 4b). The largest RMSEs for the 6-31G basis set correspond to four different systems for the training and test sets for both spin states. For the ground state, shown in Figure 4a, the largest error in the training set corresponds to the doublet state of CN with an RMSE of  $1.7559 \times 10^{-3}$  E<sub>h</sub> and, for the test set, the singlet state of C<sub>2</sub> with an RMSE of  $2.1021 \times 10^{-3} E_h$ . The excited spin states have a training RMSE of  $2.1099 \times 10^{-3} E_h$  for the doublet state of BC and test RMSE of  $2.8779 \times 10^{-3} E_h$  for the singlet state of B2. Among the ground state systems, CN has the largest training and test RMSE of  $6.5752 \times 10^{-3}$   $E_h$  and  $7.0247 \times 10^{-3}$  $E_{\rm h}$ , respectively, both of which correspond to the doublet state



**Figure 4.** Error plots for the model trained considering all available data within a given basis set where the (a) ground and (b) excited spin states are partitioned into the training (top; 50% of the data) and test set (bottom; 50% of the data).

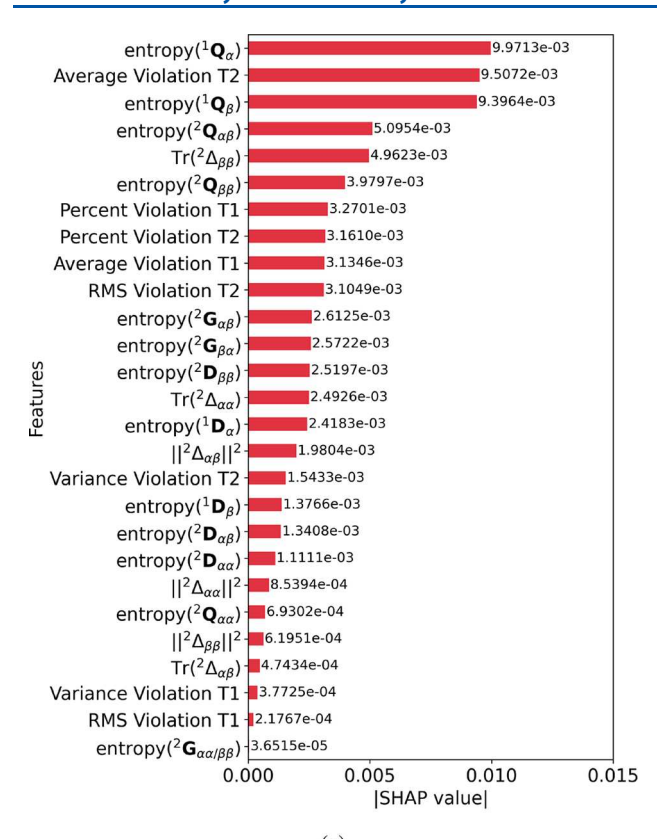
of CN at the cc-pVDZ basis set. Similar to the ground state systems, the largest training and test errors for the excited states correspond to two cc-pVDZ systems, where the training RMSE is  $5.3685 \times 10^{-3} E_{\rm h}$  for the singlet state of  $C_2$  and the test RMSE is  $4.9285 \times 10^{-3} E_{\rm h}$  for the doublet state of BC.

Lastly, we explore the issue of interpretability by investigating how the feature set affects the performance of the DDv2RDM model performance. For that purpose, we have used SHapley Additive exPlanation (SHAP) values. The SHAP analysis provides feature explanation values based on cooperative game theory that show how features (players in the game) affect the ML model in an additive manner with regard to the prior expectation value E[f(X)], where f(X) is the model target value dependent on the feature set X. As a method based on game theory, the base value of E[f(X)] corresponds to the model trained without any features (no players being present), and then, features are added into the

model such that the SHAP values of individual features always sum to the difference between all features (players) and no features (players) being present. In other words, the SHAP values will sum up to the difference between E[f(X)] and f(X). Based on this formulation, SHAP values can provide a clear measure of how strongly a feature positively or negatively impacts the model, as each SHAP value is summed from E[f(X)] to the predicted value f(X).

As a measure of feature importance, we use the absolute value of the SHAP values when analyzing single systems and the mean absolute SHAP values when analyzing sets of data. As an example, using the 6-31G basis set, we compare the absolute SHAP values of the ground spin state of the C<sub>2</sub> molecule at 1.7 Å (Figure 5a) and the mean absolute SHAP values of the full data set (Figure 5b) consisting of 17 molecules in their ground spin state and 21 molecules in their excited spin state. For both cases, the three most important features correspond to the average violation of the T2 conditions and the entropies of the  $\alpha$ - and  $\beta$ -blocks of onehole RDM (<sup>1</sup>Q). The essential role of T2 is not surprising. Violations in the T1 and T2 conditions are the only features that are directly related to energy errors (in the sense that, for an exact solution, the T1 and T2 conditions would not be violated), and T2 is known to be the stronger condition. On the other hand, the importance of the entropy of the one-hole RDM was not anticipated, nor was the fact that the entropy of the 1RDM apparently contains much less valuable information for the model. <sup>1</sup>D and <sup>1</sup>Q have complementary structures, so it is not immediately obvious why one of these RDMs would contain more useful information than the other. Nevertheless, the SHAP values clearly indicate that the entropy of <sup>1</sup>Q significantly impacts the model performance.

Among the features that have less impact on the model performance, a few are worth highlighting. First, as shown in Figure 5a,b, the variance of the violations of the T1 condition and the RMS violations in the T1 condition are clearly not important. The average violation in the T1 condition carries slightly more weight in the model, but this feature is still far less impactful than the entropy of <sup>1</sup>Q or the average violation in the T2 condition. While violations in the T1 condition imply that the 2RDM is not N-representable and, thus, that the associated energy is a lower bound to the CI energy, it is wellknown that T1 is a weak condition, compared to T2. From this point of view, it is not too surprising that violations in T1 do not carry much important information for the model. Second, for the full set of data in the 6-31G basis set (Figure 5b), the least important feature is the trace of the  $\alpha\beta$ -block of  $^2\Delta$ ; this feature is also unimportant for the specific case of the ground spin state of C<sub>2</sub> (Figure 5a). It can be shown that the trace of the full cumulant 2RDM is negative for a correlated system; it can also be shown that the trace of the  $\alpha\beta$ -block of  $^2\Delta$  should be exactly zero. However, in practice, we obtain small nonzero values for  $Tr(^2\Delta_{\alpha\beta})$  that reflect the convergence criteria we use in the v2RDM optimization. We have intentionally included these small, nonphysical quantities in our model as a means of testing the ability of SHAP analysis to identify irrelevant features. Indeed, the SHAP values clearly and correctly reflect that this feature does not impact the ML model, which suggests that this sort of analysis could be used for more elaborate feature engineering. When retraining the model in the absence of the  $Tr(^2\Delta_{\alpha\beta})$  feature, we obtain incrementally improved results, with less overfitting. This reduction in overfitting is highlighted by reduction of the absolute deviation



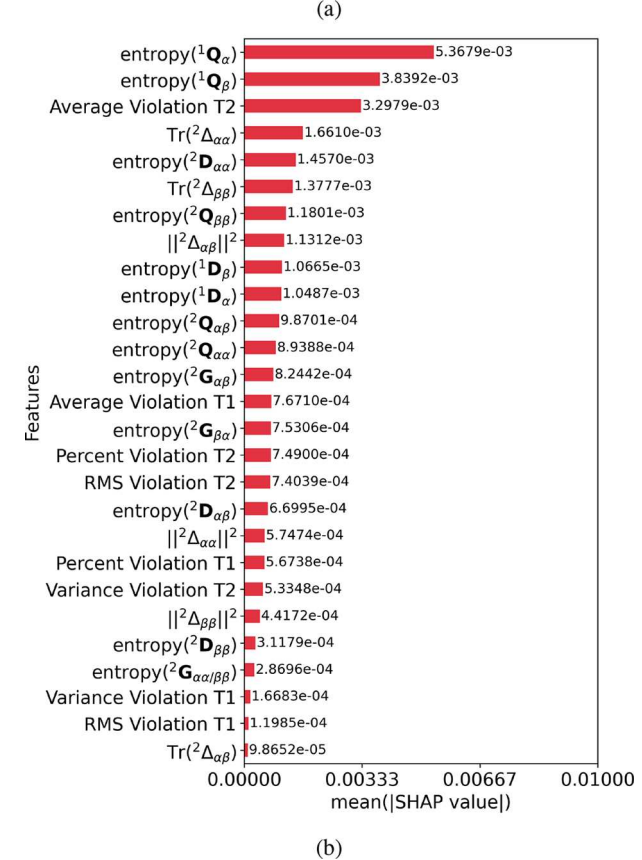


**Figure 5.** SHAP values in the form of bar graphs for (a) the molecule with the maximum deviation (ground state of  $C_2$  with the 6-31G basis set and at 1.7 Å) and (b) all the molecules obtained with the 6-31G basis set.

between train and test RMSEs of  $4.6253 \times 10^{-4} E_h$  of the original model and  $3.4936 \times 10^{-4} E_h$  for the updated model (see Figure S66).

The trends highlighted for the 6-31G data set from the SHAP analysis are consistent with those observed in the STO-3G (Figure S63) and cc-pVDZ (Figure S64) data sets, which are compared with the 6-31G data in Figure S65. As discussed above, the average violation of T2 is among the most important features in the STO-3G and cc-pVDZ models (actually, according to the SHAP analysis, it is the most important feature in these models), and the entropies of  ${}^{1}\mathbf{Q}_{\alpha}$ and  ${}^{1}\mathbf{Q}_{\beta}$  are also among the three most important features for the STO-3G data set. For the cc-pVDZ data set, only the entropy of <sup>1</sup>Q<sub>B</sub> appears among the three most important features. As depicted in Figure S65 we can also see that  $Tr(^2\Delta_{\alpha\beta})$  and violations of the T1 condition are, again, among the least important features in the data sets. Overall, the SHAP values appear to be useful for providing insights into the relationships between the physical information introduced through the DDv2RDM feature set and the target value.

To summarize, we have introduced a data-driven v2RDMbased method, DDv2RDM, which is an ML model for the efficient recovery of CI-quality electronic energies. Using a diverse data set composed of diatomic species in multiple spin states and basis sets, our models exhibit mean RMSEs of  $1.4443\times10^{-3}$  to  $1.7841\times10^{-3}~E_{\rm h}$  which is near chemical accuracy (i.e.,  $1.5936\times10^{-3}~E_{\rm h}$  or 1 kcal/mol) and a significant improvement over the native accuracy of v2RDM calculations performed under two-body N-representability conditions. A crucial component of the success of this model is the use of features based on high-order N-representability conditions (T2) evaluated with knowledge of RDMs that can be optimized efficiently using low-order v2RDM theory. We also introduced SHAP value analysis, a feature importance method based on cooperative game theory that can provide insights into the physical information included in the feature set and the impact of these features on the ability of the model to learn the v2RDM energy correction. The insights provided by this method confirmed our expectation that violations in the T2 condition carry important information that could be exploited by the ML model while also revealing the surprising impact of the entropy of the one-hole RDM on the model. This work paves the way for improved ML models that refine energy estimates from v2RDM theory and provide highaccuracy alternatives to intractable CI-based calculations on large numbers of strongly correlated electrons.

#### ASSOCIATED CONTENT

#### Supporting Information

The Supporting Information is available free of charge at https://pubs.acs.org/doi/10.1021/acs.jpclett.3c01382.

Energies for different spin states, model parameters, error analysis, dissociation curves and corrections for each diatomic molecule, and SHAP details (PDF)

#### AUTHOR INFORMATION

#### **Corresponding Authors**

A. Eugene DePrince, III — Department of Chemistry and Biochemistry, Florida State University, Tallahassee, Florida 32306-4390, United States; orcid.org/0000-0003-1061-2521; Email: adeprince@fsu.edu

Konstantinos D. Vogiatzis — Department of Chemistry, University of Tennessee, Knoxville, Tennessee 37996, United States; orcid.org/0000-0002-7439-3850; Email: kvogiatz@utk.edu

#### **Authors**

Grier M. Jones — Department of Chemistry, University of Tennessee, Knoxville, Tennessee 37996, United States; orcid.org/0000-0002-1895-0296

Run R. Li – Department of Chemistry and Biochemistry, Florida State University, Tallahassee, Florida 32306-4390, United States; orcid.org/0000-0002-3349-3169

Complete contact information is available at: https://pubs.acs.org/10.1021/acs.jpclett.3c01382

#### Notes

The authors declare no competing financial interest.

#### ACKNOWLEDGMENTS

This material is based upon work supported by the U.S. Department of Energy, Office of Science, Office of Advanced Scientific Computing Research and Office of Basic Energy Sciences, Scientific Discovery through the Advanced Computing (SciDAC) program under Award No. DE-SC0022263. This material is based on work supported by the National Science Foundation (NSF CAREER Award) under Grant CHE-2143354 (G.M.J. and K.D.V.).

#### REFERENCES

- (1) Roos, B. O.; Taylor, P. R.; Sigbahn, P. E. M. A complete active space SCF method (CASSCF) using a density matrix formulated super-CI approach. *Chem. Phys.* **1980**, *48*, 157–173.
- (2) Siegbahn, P.; Heiberg, A.; Roos, B.; Levy, B. A comparison of the super-CI and the Newton–Raphson scheme in the complete active space SCF method. *Phys. Scr.* **1980**, *21*, 323–327.
- (3) Siegbahn, P. E. M.; Almlöf, J.; Heiberg, A.; Roos, B. O. The complete active space SCF (CASSCF) method in Newton–Raphson formulation with application to the HNO molecule. *J. Chem. Phys.* **1981**, *74*, 2384–2396.
- (4) Roos, B. O. Advances in Chemical Physics; Ab Initio Methods in Quantum Chemistry Part 2; John Wiley and Sons, Ltd., 1987; Vol. 69, pp 399–445.
- (5) Vogiatzis, K. D.; Ma, D.; Olsen, J.; Gagliardi, L.; de Jong, W. A. Pushing configuration-interaction to the limit: Towards massively parallel MCSCF calculations. *J. Chem. Phys.* **2017**, *147*, 184111.
- (6) Olsen, J.; Roos, B. O.; et al. Determinant based configuration interaction algorithms for complete and restricted configuration interaction spaces. *J. Chem. Phys.* 1988, 89, 2185–2192.
- (7) Malmqvist, P. A.; Rendell, A.; Roos, B. O. The restricted active space self-consistent-field method, implementation with a split graph unitary group approach. *J. Phys. Chem.* **1990**, *94*, 5477–5482.
- (8) Fleig, T.; Olsen, J.; Marian, C. M. The generalized active space concept for the relativistic treatment of electron correlation. I. Kramers-restricted two-component configuration interaction. *J. Chem. Phys.* **2001**, *114*, 4775–4790.
- (9) Ma, D.; Li Manni, G.; Gagliardi, L. The generalized active space concept in multiconfigurational self-consistent field methods. *J. Chem. Phys.* **2011**, *135*, No. 044128.
- (10) Li Manni, G.; Ma, D.; Aquilante, F.; Olsen, J.; Gagliardi, L. SplitGAS for strong correlation and the challenging case of Cr<sub>2</sub>. *J. Chem. Theory Comput.* **2013**, *9*, 3375–3384.
- (11) Thomas, R. E.; Sun, Q.; Booth, G. H.; et al. Stochastic multiconfigurational self-consistent field theory. *J. Chem. Theory Comput.* **2015**, *11*, 5316.
- (12) Li Manni, G.; Smart, S. D.; Alavi, A. Combining the complete active space self-consistent field method and the full configuration

- interaction quantum monte carlo within a super-CI framework, with application to challenging metal-porphyrins. *J. Chem. Theory Comput.* **2016**, *12*, 1245.
- (13) Levine, D. S.; Hait, D.; Tubman, N. M.; Lehtola, S.; Whaley, K. B.; Head-Gordon, M. CASSCF with Extremely Large Active Spaces Using the Adaptive Sampling Configuration Interaction Method. *J. Chem. Theory Comput.* **2020**, *16*, 2340–2354.
- (14) Schriber, J. B.; Evangelista, F. A. Communication: An adaptive configuration interaction approach for strongly correlated electrons with tunable accuracy. *J. Chem. Phys.* **2016**, *144*, 161106.
- (15) Ghosh, D.; Hachmann, J.; Yanai, T.; Chan, G. K.-L. Orbital optimization in the density matrix renormalization group, with applications to polyenes and  $\beta$ -carotene. *J. Chem. Phys.* **2008**, *128*, 144117.
- (16) Yanai, T.; Kurashige, Y.; Ghosh, D.; Chan, G. K.-L. Accelerating convergence in iterative solution for large-scale complete active space self-consistent-field calculations. *Int. J. Quantum Chem.* **2009**, *109*, 2178–2190.
- (17) Wouters, S.; Poelmans, W.; Ayers, P. W.; Van Neck, D. CheMPS2: A free open-source spin-adapted implementation of the density matrix renormalization group for ab initio quantum chemistry. *Comput. Phys. Commun.* **2014**, *185*, 1501–1514.
- (18) Sun, Q.; Yang, J.; Chan, G. K.-L. A general second order complete active space self-consistent-field solver for large-scale systems. *Chem. Phys. Lett.* **2017**, *6*83, 291–299.
- (19) Ma, Y.; Knecht, S.; Keller, S.; Reiher, M. Second-order self-consistent-field density-matrix renormalization group. *J. Chem. Theory Comput.* **2017**, *13*, 2533–2549.
- (20) Gidofalvi, G.; Mazziotti, D. A. Active-space two-electron reduced-density-matrix method: Complete active-space calculations without diagonalization of the *N*-electron Hamiltonian. *J. Chem. Phys.* **2008**, *129*, 134108.
- (21) Fosso-Tande, J.; Nguyen, T.-S.; Gidofalvi, G.; DePrince, A. E. Large-Scale Variational Two-Electron Reduced-Density-Matrix-Driven Complete Active Space Self-Consistent Field Methods. *J. Chem. Theory Comput.* **2016**, *12*, 2260–2271.
- (22) van Aggelen, H.; Bultinck, P.; Verstichel, B.; Van Neck, D.; Ayers, P. W. Incorrect diatomic dissociation in variational reduced density matrix theory arises from the flawed description of fractionally charged atoms. *Phys. Chem. Chem. Phys.* **2009**, *11*, 5558–5560.
- (23) Verstichel, B.; van Aggelen, H.; Van Neck, D.; Ayers, P. W.; Bultinck, P. Subsystem constraints in variational second order density matrix optimization: Curing the dissociative behavior. *J. Chem. Phys.* **2010**, *132*, 114113.
- (24) van Aggelen, H.; Verstichel, B.; Bultinck, P.; Van Neck, D.; Ayers, P. W.; Cooper, D. L. Variational second order density matrix study of  $F_3^-$ : Importance of subspace constraints for size-consistency. *J. Chem. Phys.* **2011**, *134*, No. 054115.
- (25) van Aggelen, H.; Verstichel, B.; Bultinck, P.; Van Neck, D.; Ayers, P. W. Considerations on describing non-singlet spin states in variational second order density matrix methods. *J. Chem. Phys.* **2012**, *136*, No. 014110.
- (26) Li, R. R.; DePrince, A. E. Orbital angular momentum constraints in the variational optimization of the two-electron reduced-density matrix. *Phys. Rev. A* **2019**, *100*, No. 032509.
- (27) Li, R. R.; Rubin, N. C.; DePrince, A. E. Challenges for variational reduced-density-matrix theory: Total angular momentum constraints. *J. Chem. Theory Comput.* **2022**, *18*, 5966–5977.
- (28) Coleman, A. J. Structure of Fermion Density Matrices. Rev. Mod. Phys. 1963, 35, 668-686.
- (29) Mazziotti, D. A. Structure of fermionic density matrices: Complete *N*-representability conditions. *Phys. Rev. Lett.* **2012**, *108*, 263002.
- (30) Mazziotti, D. A. Significant conditions for the two-electron reduced density matrix from the constructive solution of Nrepresentability. *Phys. Rev. A* **2012**, *85*, No. 062507.
- (31) Mazziotti, D. A. Quantum Many-Body Theory from a Solution of the N-Representability Problem. *Phys. Rev. Lett.* **2023**, *130*, 153001.

- (32) Husimi, K. Some formal properties of the density matrix. *Proc. Phys.-Math. Soc. Jpn. 3rd Series* **1940**, 22, 264–314.
- (33) Löwdin, P.-O. Quantum theory of many-particle systems. I. Physical interpretations by means of density matrices, natural spin-orbitals, and convergence problems in the method of configurational interaction. *Phys. Rev.* **1955**, *97*, 1474–1489.
- (34) Mayer, J. E. Electron correlation. *Phys. Rev.* **1955**, *100*, 1579–1586.
- (35) Garrod, C.; Percus, J. K. Reduction of the *N*-particle variational problem. *J. Math. Phys.* **1964**, *5*, 1756–1776.
- (36) Garrod, C.; Mihailović, M. V.; Rosina, M. The variational approach to the two-body density matrix. *J. Math. Phys.* **1975**, *16*, 868–874
- (37) Mihailović, M. V.; Rosina, M. Variational approach to the density matrix for light nuclei. *Nucl. Phys. A* **1975**, 237, 221–228.
- (38) Rosina, M.; Garrod, C. Variational calculation of reduced density matrices. *J. Comput. Phys.* **1975**, *18*, 300–310.
- (39) Erdahl, R. M.; Garrod, C.; Golli, B.; Rosina, M. The application of group theory to generate new representability conditions for rotationally invariant density matrices. *J. Math. Phys.* **1979**, *20*, 1366–1374.
- (40) Erdahl, R. M. Two algorithms for the lower bound method of reduced density matrix theory. *Rep. Math. Phys.* **1979**, *15*, 147–162.
- (41) Nakata, M.; Nakatsuji, H.; Ehara, M.; Fukuda, M.; Nakata, K.; Fujisawa, K. Variational calculations of fermion second-order reduced density matrices by semidefinite programming algorithm. *J. Chem. Phys.* **2001**, *114*, 8282–8292.
- (42) Mazziotti, D. A. Variational minimization of atomic and molecular ground-state energies via the two-particle reduced density matrix. *Phys. Rev. A* **2002**, *65*, No. 062511.
- (43) Mazziotti, D. A. Variational reduced-density-matrix method using three-particle *N*-representability conditions with application to many-electron molecules. *Phys. Rev. A* **2006**, *74*, No. 032501.
- (44) Zhao, Z.; Braams, B. J.; Fukuda, M.; Overton, M. L.; Percus, J. K. The reduced density matrix method for electronic structure calculations and the role of three-index representability conditions. *J. Chem. Phys.* **2004**, *120*, 2095–2104.
- (45) Fukuda, M.; Braams, B. J.; Nakata, M.; Overton, M. L.; Percus, J. K.; Yamashita, M.; Zhao, Z. Large-scale semidefinite programs in electronic structure calculations. *Math. Program.* **2007**, *109*, 553–580.
- (46) Cancès, E.; Stoltz, G.; Lewin, M. The electronic ground-state energy problem: A new reduced density matrix approach. *J. Chem. Phys.* **2006**, 125, No. 064101.
- (47) Verstichel, B.; Aggelen, H. V.; Neck, D. V.; Ayers, P. W.; Bultinck, P. Variational determination of the second-order density matrix for the isoelectronic series of beryllium, neon, and silicon. *Phys. Rev. A* **2009**, *80*, No. 032508.
- (48) Fosso-Tande, J.; Nascimento, D. R.; DePrince, A. E. Accuracy of two-particle *N*-representability conditions for describing different spin states and the singlet-triplet gap in the linear acene series. *Mol. Phys.* **2016**, *114*, 423–430.
- (49) Verstichel, B.; van Aggelen, H.; Van Neck, D.; Bultinck, P.; Baerdemacker, S. D. A primal-dual semidefinite programming algorithm tailored to the variational determination of the two-body density matrix. *Comput. Phys. Commun.* **2011**, *182*, 1235–1244.
- (50) Pelzer, K.; Greenman, L.; Gidofalvi, G.; Mazziotti, D. A. Strong Correlation in Acene Sheets from the Active-Space Variational Two-Electron Reduced Density Matrix Method: Effects of Symmetry and Size. *J. Phys. Chem. A* **2011**, *115*, 5632–5640.
- (51) Poelmans, W.; Van Raemdonck, M.; Verstichel, B.; De Baerdemacker, S.; Torre, A.; Lain, L.; Massaccesi, G. E.; Alcoba, D. R.; Bultinck, P.; Van Neck, D. Variational optimization of the second-order density matrix corresponding to a seniority-zero configuration interaction wave function. *J. Chem. Theory Comput.* **2015**, *11*, 4064–4076.
- (52) Alcoba, D. R.; Torre, A.; Lain, L.; Massaccesi, G. E.; Oña, O. B.; Honoré, E. M.; Poelmans, W.; Van Neck, D.; Bultinck, P.; De Baerdemacker, S. Direct variational determination of the two-electron reduced density matrix for doubly occupied-configuration-interaction

- wave functions: The influence of three-index N-representability conditions. J. Chem. Phys. 2018, 148, No. 024105.
- (53) Head-Marsden, K.; Mazziotti, D. A. Pair 2-electron reduced density matrix theory using localized orbitals. *J. Chem. Phys.* **2017**, 147, No. 084101.
- (54) Mazziotti, D. A. Enhanced Constraints for Accurate Lower Bounds on Many-Electron Quantum Energies from Variational Two-Electron Reduced Density Matrix Theory. *Phys. Rev. Lett.* **2016**, *117*, 153001.
- (55) Mullinax, J. W.; Maradzike, E.; Koulias, L. N.; Mostafanejad, M.; Epifanovsky, E.; Gidofalvi, G.; DePrince, A. E. Heterogeneous CPU + GPU Algorithm for Variational Two-Electron Reduced-Density Matrix-Driven Complete Active-Space Self-Consistent Field Theory. J. Chem. Theory Comput. 2019, 15, 6164–6178.
- (56) Xie, J.; et al. Intrinsic glassy-metallic transport in an amorphous coordination polymer. *Nature* **2022**, *611*, 479–484.
- (57) Erdahl, R. M. Representability. Int. J. Quantum Chem. 1978, 13, 697-718.
- (58) Naftchi-Ardebili, K.; Hau, N. W.; Mazziotti, D. A. Rank restriction for the variational calculation of two-electron reduced density matrices of many-electron atoms and molecules. *Phys. Rev. A* **2011**, *84*, No. 052506.
- (59) Li, R. R.; Liebenthal, M.; DePrince, A. E. Challenges for variational reduced-density-matrix theory with three-particle N-representability conditions. *J. Chem. Phys.* **2021**, *155*, 174110.
- (60) Ramakrishnan, R.; Dral, P. O.; Rupp, M.; Von Lilienfeld, O. A. Big data meets quantum chemistry approximations: the  $\Delta$ -machine learning approach. *J. Chem. Theory Comput.* **2015**, *11*, 2087–2096.
- (61) Schütt, K. T.; Sauceda, H. E.; Kindermans, P.-J.; Tkatchenko, A.; Müller, K.-R. Schnet—a deep learning architecture for molecules and materials. *J. Chem. Phys.* **2018**, *148*, 241722.
- (62) Welborn, M.; Cheng, L.; Miller, T. F. Transferability in Machine Learning for Electronic Structure via the Molecular Orbital Basis. J. Chem. Theory Comput. 2018, 14, 4772–4779.
- (63) Cheng, L.; Welborn, M.; Christensen, A. S.; Miller, T. F. A universal density matrix functional from molecular orbital-based machine learning: Transferability across organic molecules. *J. Chem. Phys.* **2019**, *150*, 131103.
- (64) Cheng, L.; Kovachki, N. B.; Welborn, M.; Miller, T. F. Regression clustering for improved accuracy and training costs with molecular-orbital-based machine learning. *J. Chem. Theory Comput.* **2019**, *15*, 6668–6677.
- (65) Townsend, J.; Vogiatzis, K. D. Transferable MP2-Based Machine Learning for Accurate Coupled-Cluster Energies. *J. Chem. Theory Comput.* **2020**, *16*, 7453–7461.
- (66) Husch, T.; Sun, J.; Cheng, L.; Lee, S. J.; Miller, T. F. Improved accuracy and transferability of molecular-orbital-based machine learning: Organics, transition-metal complexes, non-covalent interactions, and transition states. *J. Chem. Phys.* **2021**, *154*, No. 064108.
- (67) Jones, G. M.; Pathirage, P. V. S.; Vogiatzis, K. D. Quantum Chemistry in the Age of Machine Learning; Elsevier, 2023; pp 509–529.
- (68) Townsend, J.; Vogiatzis, K. D. Data-driven acceleration of the coupled-cluster singles and doubles iterative solver. *J. Phys. Chem. Lett.* **2019**, *10*, 4129–4135.
- (69) Hermann, J.; Schätzle, Z.; Noé, F. Deep-neural-network solution of the electronic Schrödinger equation. *Nat. Chem.* **2020**, 12, 891–897.
- (70) Dral, P. O., Ed.; Quantum Chemistry in the Age of Machine Learning; 2023.
- (71) Chen, Y.; Ou, Y.; Zheng, P.; Huang, Y.; Ge, F.; Dral, P. O. Benchmark of general-purpose machine learning-based quantum mechanical method AIQM1 on reaction barrier heights. *J. Chem. Phys.* **2023**, *158*, No. 074103.
- (72) Coe, J. P. Machine learning configuration interaction. *J. Chem. Theory Comput.* **2018**, *14*, 5739–5749.
- (73) Coe, J. P. Machine learning configuration interaction for ab initio potential energy curves. *J. Chem. Theory Comput.* **2019**, *15*, 6179–6189.

- (74) Yang, P.-J.; Sugiyama, M.; Tsuda, K.; Yanai, T. Artificial neural networks applied as molecular wave function solvers. *J. Chem. Theory Comput.* **2020**, *16*, 3513–3529.
- (75) Pineda Flores, S. D. Chembot: a machine learning approach to selective configuration interaction. *J. Chem. Theory Comput.* **2021**, *17*, 4028–4038.
- (76) Jeong, W.; Gaggioli, C. A.; Gagliardi, L. Active learning configuration interaction for excited-state calculations of polycyclic aromatic hydrocarbons. *J. Chem. Theory Comput.* **2021**, *17*, 7518–7530.
- (77) Peyton, B. G.; Briggs, C.; D'Cunha, R.; Margraf, J. T.; Crawford, T. D. Machine-learning coupled cluster properties through a density tensor representation. *J. Phys. Chem. A* **2020**, *124*, 4861–4871.
- (78) Sager-Smith, L. M.; Mazziotti, D. A. Reducing the Quantum Many-Electron Problem to Two Electrons with Machine Learning. *J. Am. Chem. Soc.* **2022**, *144*, 18959–18966.
- (79) Mazziotti, D. A. Approximate solution for electron correlation through the use of Schwinger probes. *Chem. Phys. Lett.* **1998**, 289, 419–427.
- (80) Pedregosa, F.; Varoquaux, G.; Gramfort, A.; Michel, V.; Thirion, B.; Grisel, O.; Blondel, M.; Prettenhofer, P.; Weiss, R.; Dubourg, V. Scikit-learn: Machine learning in Python. *J. Mach. Learn. Res.* **2011**, *12*, 2825–2830.
- (81) Lundberg, S. M.; Lee, S.-I. In *Advances in Neural Information Processing Systems* 30; Guyon, I., Luxburg, U. V., Bengio, S., Wallach, H., Fergus, R., Vishwanathan, S., Garnett, R., Eds.; Curran Associates, Inc., 2017; pp 4765–4774.

### TRecommended by ACS

#### **Periodic Bootstrap Embedding**

Oinam Romesh Meitei and Troy Van Voorhis

MAY 08, 2023

JOURNAL OF CHEMICAL THEORY AND COMPUTATION

READ 🗹

### Riemannian Trust Region Method for Minimization of the Fourth Central Moment for Localized Molecular Orbitals

Aliakbar Sepehri, Mark R. Hoffmann, et al.

JUNE 07, 2023

THE JOURNAL OF PHYSICAL CHEMISTRY A

READ 🗹

## Efficient All-Electron Time-Dependent Density Functional Theory Calculations Using an Enriched Finite Element Basis

Bikash Kanungo, Vikram Gavini, et al.

JANUARY 19, 2023

JOURNAL OF CHEMICAL THEORY AND COMPUTATION

READ 🗹

### Toward Chemical Accuracy Using the Jastrow Correlated Antisymmetrized Geminal Power Ansatz

Abhishek Raghav, Kousuke Nakano, et al.

APRIL 04, 2023

JOURNAL OF CHEMICAL THEORY AND COMPUTATION

READ 🗹

Get More Suggestions >